The Influence of Extratropical Ocean on the PNA Teleconnection: Role of Atmosphere‐Ocean Coupling

Mori, Masato
Research Institute for Applied Mechanics, Kyushu University

Tokinaga, Hiroki
Research Institute for Applied Mechanics, Kyushu University

Kosaka, Yu
Research Center for Advanced Science and Technology, the University of Tokyo

Nakamura, Hisashi
Research Center for Advanced Science and Technology, the University of Tokyo

他

https://hdl.handle.net/2324/7348045

出版情報：Geophysical Research Letters. 51 (14), pp.e2024GL110234-, 2024-07-15. American Geophysical Union (AGU)
バージョン：

ADVANCING EARTH AND SPACE SCIENCES

Geophysical Research Letters

RESEARCH LETTER
10.1029/2024GL110234

Key Points:

- Extratropical air-sea coupling enhances the variance of the Pacific/North American (PNA) pattern, which explains 16% of the total variance
- The enhancement is due to the reduced damping of available potential energy through modulations of turbulent heat fluxes and precipitation
- Atmosphere-only simulation is likely to underestimate the impact of extratropical sea surface temperature anomalies on the PNA variability

Supporting Information:

Supporting Information may be found in the online version of this article.

Correspondence to:

M. Mori,
masato@riam.kyushu-u.ac.jp

Citation:

Mori, M., Tokinaga, H., Kosaka, Y., Nakamura, H., Taguchi, B., & Tatebe, H. (2024). The influence of extratropical ocean on the PNA teleconnection: Role of atmosphere-ocean coupling. *Geophysical Research Letters*, *51*, e2024GL110234. https://doi.org/10.1029/2024GL110234

Received 10 MAY 2024
Accepted 5 JUL 2024

The Influence of Extratropical Ocean on the PNA Teleconnection: Role of Atmosphere-Ocean Coupling

Masato Mori[1], Hiroki Tokinaga[1], Yu Kosaka[2], Hisashi Nakamura[2], Bunmei Taguchi[3], and Hiroaki Tatebe[4]

[1]Research Institute for Applied Mechanics, Kyushu University, Kasuga, Japan, [2]Research Center for Advanced Science and Technology, the University of Tokyo, Tokyo, Japan, [3]Faculty of Sustainable Design, University of Toyama, Toyama, Japan, [4]Japan Agency for Marine-Earth Science and Technology, Yokohama, Japan

Abstract The Pacific/North American (PNA) pattern is a major low-frequency variability in boreal winter. A recent modeling study suggested that PNA variability increases through extratropical atmosphere-ocean coupling, but the effect was not fully extracted due to a particular experimental design. By comparing coupled and two sets of uncoupled large-ensemble global model simulations, here we show that the PNA-induced horseshoe-shaped sea-surface temperature (SST) anomaly in the North Pacific returns a non-negligible influence on the PNA itself. Its magnitude depends on the presence or absence of atmosphere-ocean coupling. The coupling accounts for ∼16% of the PNA variance, while the horseshoe-shaped SST anomaly explains only 5% under the uncoupled condition. The coupling reduces the damping of available potential energy by modulating turbulent heat fluxes and precipitation, magnifying the PNA variance. Precipitation processes in the extratropics as well as tropics are therefore important for realistically representing PNA variability and thereby regional weather and climate.

Plain Language Summary Atmospheric flow is not entirely random; patterns of circulation variability appear recurrently in the same regions, known as teleconnection patterns. A major wintertime teleconnection pattern over the North Pacific-North American sector is called the Pacific/North American (PNA) pattern. It causes strong fluctuations in precipitation, air temperature, and pressure over North America through persistent strengthening or meandering of the jet stream. While the influence of tropical ocean variability, such as El Niño/La Niña, on the formation and persistence of the PNA has been known, the role of the extratropical ocean remains unclear. Here we perform a vast number of numerical model simulations to detect the influence of the extratropical ocean on PNA. We show that the atmosphere-ocean coupling (two-way interaction between the ocean and atmosphere) enhances the PNA variability (i.e., the magnitude of meandering and strengthening of the westerlies) compared to the uncoupled condition. Furthermore, we propose possible mechanisms behind this enhancement. The findings of this study are expected to contribute to improving the accuracy of long-term forecasts, such as one-month predictions, and reducing uncertainty in future climate change projections through the improvement of numerical models.

1. Introduction

The Pacific/North American (PNA) pattern is one of the most prominent atmospheric low-frequency variability in the wintertime Northern Hemisphere (Wallace & Gutzler, 1981), often causing extreme weather and climate, particularly over North America through a persistent strengthening or meandering of the jet stream (e.g., Leathers et al., 1991). The existence of the PNA pattern is suggested owing to the dynamics inherent in the extratropical atmosphere, such as barotropic energy conversion from the zonally asymmetric climatological flow (e.g., Branstator, 1990; Nakamura et al., 1987; Simmons et al., 1983) and high-frequency transient eddy feedback (e.g., Lau, 1988; Jin et al., 2006a, Jin et al., 2006b). External forcings from the tropics, represented by the El Niño-Southern Oscillation (ENSO), are known to have a profound impact on the prominence of the PNA (e.g., Horel & Wallace, 1981; Mori & Watanabe, 2008; Palmer, 1999; Trenberth et al., 1998).

The question of what role the extratropical ocean plays in the formation and maintenance of the PNA has attracted researchers for many years (Alexander et al., 2002; Bladé, 1999; Lau and Nath, 1996, 2001). Basin-scale sea-surface temperature (SST) variations in the extratropics are known to be forced primarily by the atmosphere (e.g., Alexander, 1992; Cayan, 1992b; Deser & Timlin, 1997). Vigorous internal variability of the extratropical atmosphere has thus hindered the detection of the modest impact of the extratropical ocean on the atmosphere (Kushnir et al., 2002).

Nevertheless, a recent study has tackled this issue by using large-ensemble simulation data, demonstrating that extratropical atmosphere-ocean coupling selectively enhances the variance (magnitude) of major atmospheric teleconnection patterns, including the PNA (Mori et al., 2024, hereafter M24). The surface turbulent heat flux (THF) acts to reduce air-sea temperature and humidity differences, and its magnitude becomes smaller when the basin-scale SST passively responds to overlying atmospheric anomalies than when it cannot. Therefore, in those situations where THF causes thermal damping in the atmosphere, the damping is weakened by air-sea coupling ("reduced thermal damping mechanism") (Barsugli & Battisti, 1998). By comparing general circulation model (GCM) simulations with and without air-sea coupling, M24 showed that the reduction in thermal damping due to the extratropical air-sea coupling modulates the energetics related to dynamical processes inherent in the extratropical atmosphere that characterize the PNA, resulting in increasing the available potential energy (APE) and kinetic energy (KE) associated with the PNA.

However, one critical issue remains unaddressed due to the experimental design in M24: the impact of extratropical air-sea coupling on the PNA may still be underestimated (details are described later). To resolve this issue, we reevaluate the role of the extratropical atmosphere-ocean coupling on the PNA by extending M24 with a new set of experiments where both SST and sea ice are fixed to their climatologies in the North Pacific. The new experiment is also utilized to address the question of how the PNA-forced extratropical SST anomalies return the influence on the PNA itself depending on the presence or absence of the atmosphere-ocean coupling.

2. Methods

2.1. Model Experimental Design

We use three sets of large-ensemble simulations by the sixth version of the Model for Interdisciplinary Research on Climate (MIROC6) (Tatebe et al., 2019). All three simulations are driven by the same historical external forcings and conducted for 1979–2020 with a 50-member ensemble configured with different ocean components: (a) fully coupled ocean model (CGCM) (referred to as CHIST or coupled experiment), (b) SST and sea ice obtained in CHIST are prescribed to the atmosphere-only GCM (AGCM) (referred to as AHIST), and (c) the same as in AHIST, but prescribed SST and sea ice in the North Pacific (100°E−100°W, 20°–70°N) are replaced with their climatology for 1979–2020 (referred to as ACLM). A buffer zone is set over 15°–20°N where SST anomalies are linearly reduced to zero toward 20°N. Because of no interactive ocean model coupled, the latter two AGCM experiments are also referred to as uncoupled experiments. M24 compared CHIST and AHIST, whereas ACLM has been newly conducted for the present study.

The monthly mean SST, sea-ice concentration, and sea-ice thickness fields prescribed in the two uncoupled experiments are linearly interpolated into the daily fields (Taylor et al., 2000). For a given member of CHIST, we perform the corresponding member for each AHIST and ACLM experiment. Therefore, on time scales longer than a month, SST and sea-ice variations are identical among all experiments except for the North Pacific in ACLM. In contrast, the coupled and uncoupled experiments have different sub-monthly variations in SST and sea ice. In the uncoupled experiments, interpolated daily SST and sea ice vary independently of atmospheric variability, while in CHIST, they fluctuate in interacting with the atmosphere. Therefore, we can interpret the difference in the long-term statistics of atmospheric variability between the coupled and uncoupled experiments as arising from the presence of atmosphere-ocean coupling. Note the assessment of the coupling effect varies depending on which uncoupled experiment is chosen for comparison, while the differences between AHIST and ACLM can be interpreted as the impact of North Pacific SST anomalies under uncoupled conditions. Further details of the model configurations and experimental designs are given in M24.

2.2. The PNA Pattern

We analyze the December-January-February (DJF) mean anomalies from the climatology for 1980–2020 in each experiment. The PNA pattern is defined as the first mode of empirical orthogonal function (EOF) of the DJF-mean 500 hPa geopotential height (Z500) anomalies over the Pacific/North American domain (120°E–120°W, 20°–90°N), based on Lee et al. (2019). The anomalies are weighted by the square root of the cosine of latitude. The EOF analysis is applied to a concatenated series of anomalies comprising 150 members across the

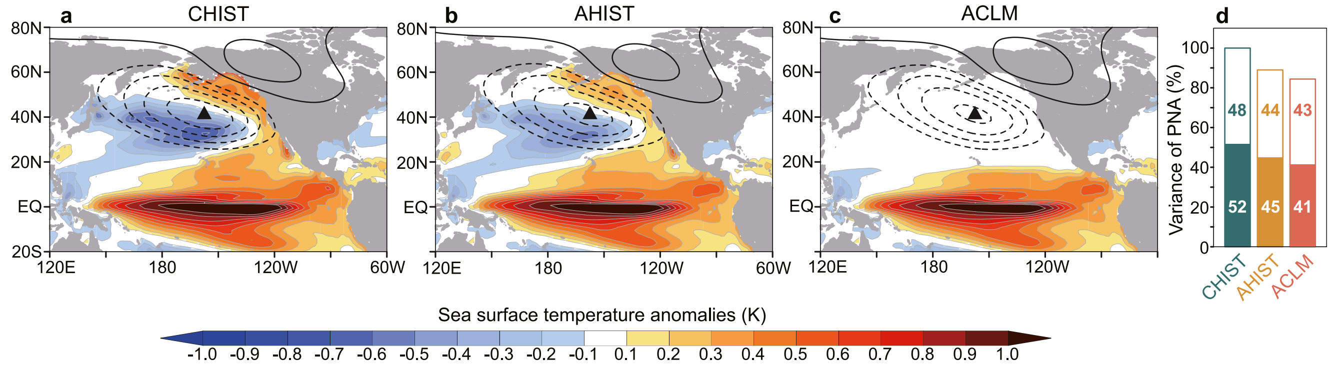

Figure 1. Different PNA patterns in three experiments. (a–c), DJF-mean anomalies of SST (shading, K) and Z500 (contours at 15 m intervals, dashed if negative) regressed on the PNA index separately for CHIST (a), AHIST (b), and ACLM (c) (colored only where the statistical confidence exceeds 99% level). Black triangle on each panel (157°W, 41°N) corresponds to the strongest negative Z500 anomaly associated with PNA. (d), Variance of PNA for each experiment. The variance explained by the ENSO-forced response and the internal variability are indicated with filled and open boxes, respectively.

experiments. The variance of the principal component in each experiment (41 winters × 50 members = 2050 samples) represents the respective PNA variance. Meanwhile, the principal components have been standardized separately and are referred to as PNA indices for the individual experiments. Then, the typical PNA-associated anomalies of variables are shown as a linear regression of local anomalies onto the respective PNA index. Therefore, the spatial structure of the PNA pattern is not strictly identical among experiments. Note that the PNA definition differs from M24, but this difference does not qualitatively affect our conclusions, highlighting robustness. Statistical tests for correlation/regression coefficients and differences in regression coefficients were performed using a two-sided Student's t-test and F-test (Snedecor & Cochran, 1989), respectively. The effect of linear detrending is small enough that we show non-detrended analysis results only.

2.3. Energetics

To understand the relative importance of different physical processes that are influential in the generation and maintenance of the PNA, energy conversion terms are evaluated for each experiment based on the quasi-geostrophic momentum and thermodynamic energy equations (Text S1 in Supporting Information S1). The DJF-mean anomalies of variables regressed on the PNA index are used to calculate each conversion term without distinguishing the PNA polarity. All terms are integrated over the extratropical Northern Hemisphere (0°–360°E, 10°–90°N) and vertically from the surface up to 100 hPa. Due to the limited data for the diabatic heating rate (Q), only 10 ensemble members for 1979–2013 are used for each experiment's diabatic APE generation term (CQ).

When comparing PNA-related energetics among experiments, we should note that energy conversion and flux terms depend on the PNA pattern's magnitude, which differs among experiments. Thus, a large value of a conversion term could be either a cause or a result of strong PNA anomalies. For a fair comparison, all energy conversion and flux terms are divided by PNA's total energy, defined as the sum of KE and APE integrated over the extratropical Northern Hemisphere (0°–360°E, 10°–90°N) from the surface up to 100 hPa. The resultant value is called "efficiency" (denoted with an asterisk) (Kosaka et al., 2009; Martineau et al., 2020; M24) and is independent of PNA magnitude.

3. Results

3.1. How Does the Air-Sea Coupling Affect the PNA?

Figure 1 shows the positive phase of the PNA pattern in Z500 anomalies and associated SST anomalies for each experiment. Tropical El Niño-like SST anomalies are common to all experiments, as part of the PNA variability is forced remotely by ENSO. In CHIST, where extratropical SST anomalies can respond to the atmospheric circulation anomalies, the PNA pattern forces horseshoe-shaped SST anomalies in the North Pacific: negative anomalies in the central North Pacific and positive anomalies along the American coast (Figure 1a) (e.g., Alexander et al., 2002; Cayan, 1992a). These extratropical and tropical SST anomalies in CHIST are prescribed as the lower-boundary condition to AHIST. Therefore, some portion of the PNA anomalies is excited by ENSO simultaneously in both CHIST and AHIST. As a result, the horseshoe-shaped SST anomalies appear to be correlated with the PNA in AHIST despite no air-sea coupling. There is a possibility that this SST anomaly resulted in an underestimation of the impact of the air-sea coupling associated with PNA (M24), and verifying this is one of the goals of this study. By contrast, in the newly conducted ACLM, no SST anomalies are found in the North Pacific (Figure 1c).

A comparison between the coupled and uncoupled experiments demonstrates that allowing air-sea coupling leads to a larger PNA magnitude (Figure 1 and Figure S1 in Supporting Information S1). Relative to CHIST, the PNA variance in AHIST and ACLM is about 89% and 84%, respectively (Figure 1d). The coupling effect explains about 16% of the PNA variance, as represented by comparing CHIST with ACLM. Thus, the coupling effect on the PNA estimated as CHIST minus AHIST in M24 was indeed underestimated. Nevertheless, this underestimation, arising from the extratropical North Pacific SST anomalies (i.e., the difference between AHIST and ACLM), accounts for only 5% of the PNA variance. Therefore, the influence of PNA-induced extratropical SST anomalies on the PNA itself is sensitive to the presence or absence of atmospheric-ocean coupling, suggesting that an atmosphere-only simulation is likely to underestimate the impact of the extratropical North Pacific SST anomalies on the PNA.

To examine the extent to which the remote influence from the tropics leads to the difference in the PNA variance among experiments, we investigate the tropical precipitation anomalies associated with PNA (Figure S2 in Supporting Information S1). At first sight the anomalous precipitation does not differ markedly between experiments, but it is slightly larger in AGCM over the Niño4 region, where SST anomalies have the highest correlation with the PNA (Table S1 in Supporting Information S1). This suggests that the PNA variance difference due to the air-sea coupling (about 11% or 16%) cannot be explained solely by the different magnitude of tropical forcing driving the PNA, highlighting the importance of extratropical air-sea coupling. Meanwhile, the correlation coefficient between the PNA and Niño4 indices is 0.72, 0.71, and 0.70 for CHIST, AHIST, and ACLM, respectively (Table S1 in Supporting Information S1), indicating that ENSO explains about half of the PNA variance in the respective experiments. The residual is regarded as the internally generated component. This decomposition, summarized in Figure 1d, suggests that both the forced PNA response and internal PNA variability are enhanced by the extratropical air-sea coupling.

Since the extratropical atmospheric internal variability is vigorous in winter, differences in the PNA variance due to underlying oceanic states are difficult to assess robustly without a vast number of samples. Indeed, the ensemble size dependence of the variance difference between CHIST and AHIST indicates that at least 35 members (1435 winters) of samples are necessary to identify the coupling effect robustly at the 99% confidence level (Figure S3a in Supporting Information S1). The required ensemble size decreases to 25 (1025 winters) when comparing CHIST and ACLM (Figure S3b in Supporting Information S1), probably due to the stronger coupling effect. As suggested by such many samples required, the coupling effect is modest, and the signal-to-noise ratio is small; this is consistent with the suggestion that the coupling effect arises from the modulation of internal- and external-PNA variabilities by the extratropical ocean. Nevertheless, the coupling effect (about 16% of the total PNA variance) is non-negligible. Meanwhile, we still need 50 members for robust detection of variance differences between the uncoupled experiments (Figure S3c in Supporting Information S1). This considerably small signal-to-noise ratio is compatible with the fact that atmospheric response to extratropical SST anomalies is inconsistent across the AGCM experiments (Kushnir et al., 2002).

3.2. How Does the Extratropical Air-Sea Interaction Change With and Without Coupling?

Next, we focus on the difference in extratropical air-sea interaction with and without coupling. Figure 2 shows anomalies of THF (sum of sensible and latent heat fluxes), 10m-wind, and 700 hPa temperature (T700) associated with positive PNA for each experiment. The anomalous Z500 and T700 are nearly in quadrature, suggesting a baroclinic structure of the lower-tropospheric anomalies (M24). Hereafter, the area (160°E−140°W, 30°–40°N) is referred to as the central Pacific. The positive PNA brings colder and drier surface airmass from the Eurasian continent into the central Pacific to promote upward THF anomalies through intensification of the climatological westerlies and air-sea differences in temperature and humidity (Figures 2a–2c).

The upward THF anomalies then act as thermal damping on the atmosphere, reducing air-sea thermal differences. In CHIST, these upward THF anomalies simultaneously lower the SST. In the uncoupled experiments, by contrast, only the atmosphere can change to reduce air-sea thermal differences because SST cannot respond to the

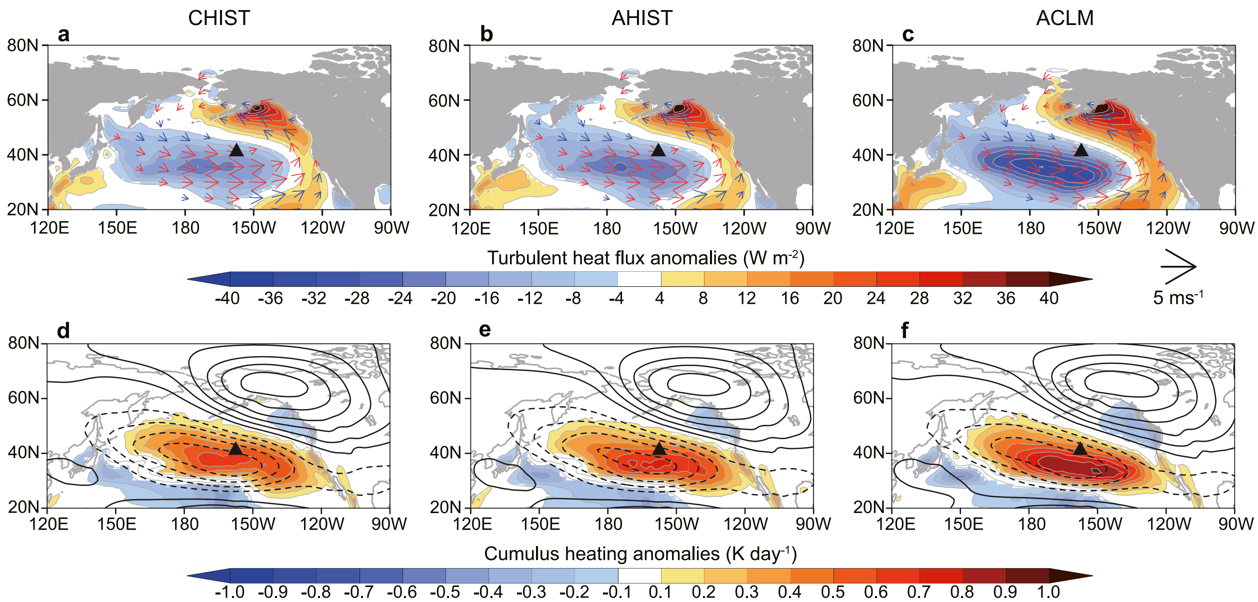

Figure 2. Different extratropical air-sea interactions in three experiments. (a–c), DJF-mean anomalies of THF (shading, downward positive, W m^{-2}) and 10 m wind (vectors, m s^{-1}) regressed on the PNA index separately for CHIST (a), AHIST (b), and ACLM (c). (d–f), Same as in panels (a–c), but for anomalous cumulus heating (shading, K day^{-1}) and temperature (contours at 0.3 K intervals, dashed if negative) at 700 hPa. Shading only where the statistical confidence exceeds 99% level. 10 m wind anomalies increasing (reducing) scalar wind speed are indicated with red (blue) vectors.

THF anomalies. As a result, excessive upward THF anomalies and thus larger thermal damping are required in the uncoupled experiments. In fact, THF anomalies become larger in AHIST than in CHIST (Figures 2a and 2b and Figure S4a in Supporting Information S1). These features become more pronounced in ACLM, where air-sea thermal differences are larger under the prescribed climatological SST (Figure 2c and Figure S4b in Supporting Information S1). These results support the reduced thermal damping mechanism (Barsugli & Battisti, 1998).

The impact of the THF anomalies on the PNA extends from the sea surface to the entire troposphere via diabatic heating (M24). Energetically, the positive (negative) covariance between anomalous diabatic heating and air temperature associated with PNA corresponds to APE generation (dissipation), expressed as the CQ term (see Equations S2 and S5 in Supporting Information S1). M24 pointed out that the anomalous diabatic heating by vertical diffusion (i.e., sensible heat flux) and cumulus/shallow convection (through latent heat flux) contribute to the APE damping (i.e., negative CQ) on the PNA at 850 hPa over the central Pacific where cold anomalies are located. At 700 hPa, the anomalous diabatic heating by cumulus convection is dominant in the central Pacific (Figures 2d–2f), with its peak located slightly downstream of the THF (mainly latent heat flux) minimum (Figures 2a–2c), showing a good agreement with the distribution of the enhanced cold airflow. Therefore, damping of APE (negative CQ) is dominant there (Figure S5a in Supporting Information S1).

Next, we investigate how the air-sea decoupling modulates the negative CQ. Note that CQ is normalized by the total energy of PNA in each experiment to exclude its dependency on the PNA magnitude. The decoupling essentially promotes APE damping, but the modifications in CQ are rather complex (Figures S5b–S5c in Supporting Information S1) mainly due to the opposing contributions between cumulus convection and large-scale condensation (LSC) to precipitation anomalies over the central Pacific (Figures S5e, S5f, S5h, and S5i in Supporting Information S1). As the upward THF anomalies are intensified in the central Pacific compared with CHIST (Figures S4a–S4b in Supporting Information S1), both cumulus precipitation (Figures 3b, 3e, and 3h) and the associated diabatic heating (Figures 2d–2f and Figures S4c–S4d in Supporting Information S1) also increase, leading to weaker cold T700 anomalies (Figures 2d–2f and Figures S4c–S4d in Supporting Information S1). Overall, the negative CQ is intensified by decoupling over the central Pacific (Figures S5d–S5f in Supporting Information S1). However, in ACLM, the intensification of downward THF anomalies east of the PNA anomaly center (marked with a triangle in the figure) reduces cumulus precipitation locally (Figure 3h), acting to offset the negative anomalies of the total CQ around (40°N, 150–120°W) (Figure S5f in Supporting Information S1).

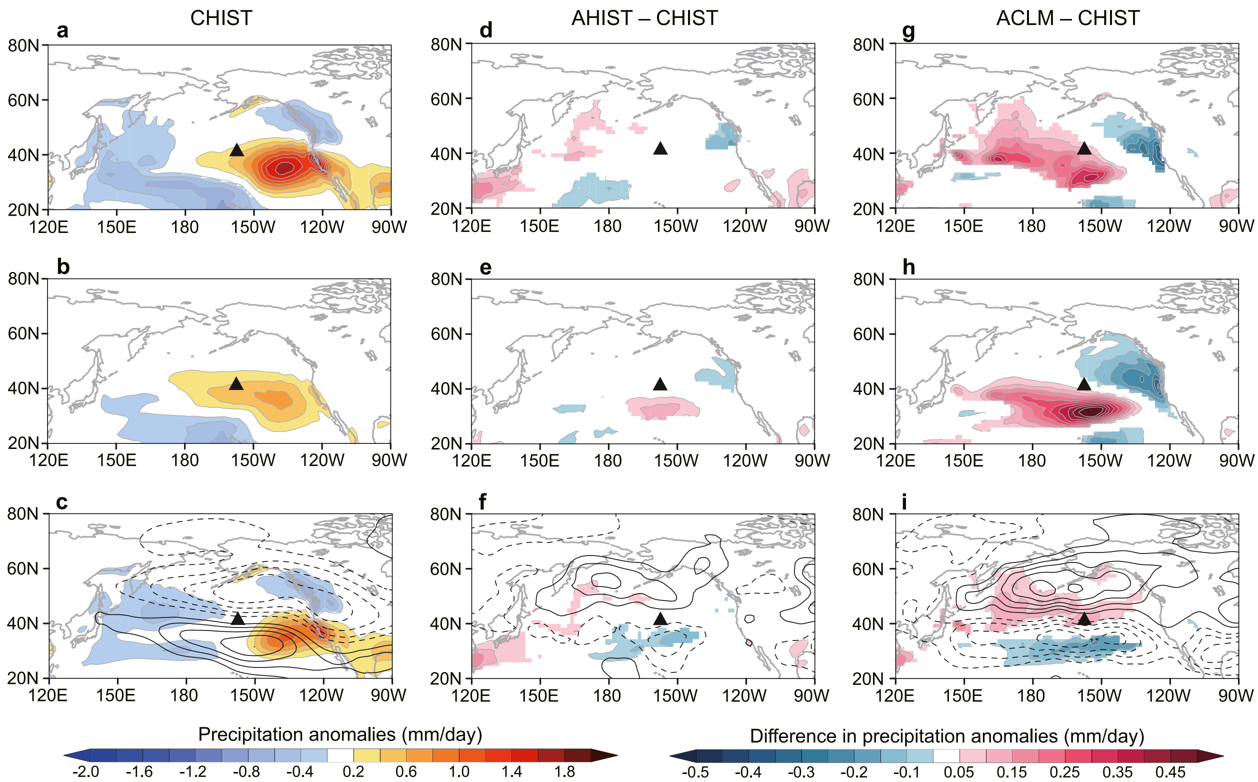

Figure 3. Comparison of precipitation anomalies between the coupled and uncoupled experiments. (a–c) DJF-mean anomalies of total precipitation (a), precipitation by cumulus (b), and by LSC (c) associated with PNA for CHIST (mm day^{-1}, colored only where the statistical confidence exceeds 99% level). (d–f) As in panels (a–c), but for the difference in AHIST from CHIST. (g–i) As in panels (a–c), but for the difference in ACLM from CHIST. Differences are shown only where the statistical confidence exceeds 95% level. Black contours (dashed if negative) represent storm-track anomalies regressed on PNA (c) (1 m intervals) and its difference from CHIST (f and i) (0.2 m intervals). The storm-track activity is defined as the standard deviation of 10-day high-pass filtered daily Z500 in DJF.

Meanwhile, the anomalous activity of the southward-displaced storm-track is weaker in the uncoupled experiments (Figures 3c, 3f, and 3i), consistent with the weakening of PNA magnitude. In response to this modulated storm-track activity, anomalous enhancement of LSC precipitation weakens over the central Pacific and its downstream (Figures 3c, 3f, and 3i), acting to reduce the negative total CQ south of 40°N (Figures S5h, S5i in Supporting Information S1). Therefore, the changes in LSC and part of cumulus convection act as brakes on APE damping. In summary, the absence of extratropical air-sea coupling intensifies the APE damping on the PNA in the lower and mid-troposphere through changes in precipitation, the extent of which depends on the condition of underlying SST anomalies and the magnitude of PNA itself.

3.3. How Does the Energetics of PNA Change by Air-Sea Coupling?

We investigate the energetics to understand how the extratropical air-sea coupling enhances the PNA variance through changes in APE damping. Barotropic energy conversion from the mean state (CK*) is the most dominant process for the maintenance of PNA (Figure 4a), consistent with previous studies (e.g., Branstator, 1990; Mori & Watanabe, 2008; Simmons et al., 1983). Yet, baroclinic energy conversion from the mean state (CP*) has a comparable contribution (Kim et al., 2021, M24), though overlooked thus far. Barotropic feedback forcing from modulated storm-track activity via eddy momentum flux (CK_{HF}*) also contributes positively to the maintenance in the upper troposphere (Lau, 1988), but its thermal effect via eddy heat flux (CP_{HF}*) acts to reduce the APE mainly in the lower troposphere (Lau & Holopainen, 1984). Therefore, the net feedback from transient eddies is relatively weak, but they contribute to forming deep PNA anomalies.

CQ* acts as the APE damping (Figure 4a), which is dominant over the entire Northern Hemisphere in all experiments and the smallest in CHIST (i.e., reduced APE damping by air-sea coupling). The modulation of the APE damping by air-sea coupling induces slight structural changes in PNA anomaly, whose effect ultimately extends to all energy conversion terms. The sum of the conversion/generation efficiencies for APE

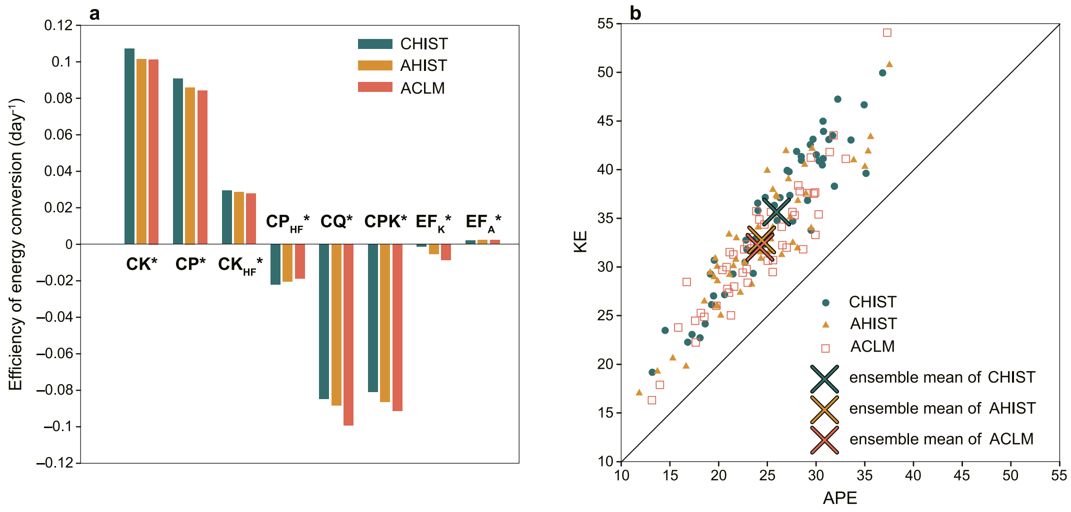

Figure 4. Difference in energetics among three experiments. (a), Efficiency of energy conversion terms (day^{-1}) associated with PNA in CHIST (green), AHIST (yellow), and ACLM (orange). CK and CP denote barotropic and baroclinic energy conversions from the climatological-mean fields, respectively, CK_{HF} and CP_{HF} barotropic and baroclinic feedbacks, respectively, from high-frequency transient eddies, CQ diabatic APE generation, CPK conversion from APE to KE, and EF_K and EF_A energy inflows across the southern boundary (10°N). (b), Scatter plot of KE and APE (units: 10^{17}J) associated with PNA for each ensemble member. Green dots, yellow triangles, and orange squares indicate CHIST, AHIST, and ACLM, respectively. Cross marks indicate the ensemble mean of individual experiments.

($CP^* + CP_{HF}^* + CQ^* + EF_A^*$) is largest (smallest) at −0.014 (−0.032) in CHIST (ACLM), which is concomitant with the smallest (largest) conversion efficiency from KE to APE (negative CPK*). This modulation in CPK* means that damping to KE in CHIST (ACLM) is the smallest (largest), which is consistent with the greatest (smallest) KE among experiments (Figure 4b). In addition, the highest CK* of CHIST also contributes to the greatest KE. The change in CK* is attributable to the slight structural changes in the PNA anomaly through the air-sea coupling rather than subtle differences in the climatological-mean state among experiments, suggesting a mechanism for the enhanced CK* due to the change in energy balance triggered by the CQ* modulation.

The efficiencies of energy fluxes across the southern boundary (EF_K* and EF_A*) are tiny (Figure 4a), but a slight increase in energy outflow (EF_K*) by decoupling contributes to the KE differences. Since the two uncoupled experiments differ only in the prescribed SST in the North Pacific, the energy outflow increase is interpreted as a result of changes in energy conversion efficiency in the extratropics rather than that of differences in influence from the tropics. In summary, the existence of extratropical air-sea coupling leads to a change in the dynamical balance governing the energy transfer within the PNA and with the time-mean flow through reduced APE damping, resulting in an increase in KE, APE, and thus the variance of PNA.

KE and APE increase to satisfy the PNA pattern-specific energy balance (M24). Figure 4b shows scatter plots of PNA-associated APE and KE obtained for individual ensemble members of each experiment. Despite a large spread of energy among members, APE and KE are highly correlated, implying that the changes in APE can lead to changes in KE and vice versa (M24). As represented by the ensemble-mean differences of KE and APE between the coupled and uncoupled experiments, the coupling causes systematic changes in the energy. The emsemble-mean increases in KE and APE are larger when CHIST is compared with ACLM than with AHIST.

4. Summary and Discussion

Extratropical basin-scale SST variations are overall passive to atmospheric variations, and the PNA pattern forces a horseshoe-shaped SST anomaly in the North Pacific. Our results suggest that the extratropical ocean also simultaneously exerts a non-negligible influence on the PNA by reducing APE damping. The extratropical atmosphere-ocean coupling thus strengthens the PNA pattern compared to the uncoupled cases. The coupling effect, estimated from the difference between CHIST and ACLM, explains about 16% of the total PNA variance. When CHIST is compared to AHIST, the coupling effect decreases to about 11% because APE damping weakens under the prescribed SST variations with the extratropical horseshoe-shaped anomaly that could intensify the

PNA. However, under the uncoupled condition, this SST impact on the PNA explains only 5% of the total PNA variance, much smaller than the coupling effect. Our comparison of the coupled and uncoupled experiments highlights for the first time that the reverse impact of the horseshoe-shaped extratropical SST anomaly on the PNA must be substantially underestimated by conventional SST-forced AGCM experiments.

The reduced APE damping by coupling is largely due to changes in precipitation processes. Therefore, the extent to which the coupling affects the PNA magnitude may be model-dependent, improvements in simulated extratropical precipitation may therefore extert a non-negligible impact on the predictability and reproducibility of the PNA. The findings of this study are also expected to have important implications for the question of how the PNA can change under the warming climate.

Conflict of Interest

The authors declare no conflicts of interest relevant to this study.

Data Availability Statement

The MIROC6 historical and SSP5-8.5 scenario simulations (referred to as CHIST in this study) are available from the Earth System Grid Federation (ESGF) archive (https://esgf-node.llnl.gov/search/cmip6/). The MIROC6 AGCM data sets are available from Zenodo (Mori, 2024a, 2024b).

Acknowledgments
The authors thank the two anonymous reviewers for their valuable comments. This work is supported by the Japan Ministry of Education, Culture, Sports, Science and Technology through the advanced studies of climate change projection (SENTAN: Grant JPMXD0722680395) program, the Arctic Challenge for Sustainability II (ArCS II: Grant JPMXD1420318865) Program, and by the Japan Society for the Promotion of Science through KAKENHI Grants JP19H05702, JP19H05704, JP22H01292, JP23K22563, JP23K22570, JP23K25937, JP23K25946, JP24H02223, JP24H02229, and JP24K07134.

References

Alexander, M. A. (1992). Midlatitude atmosphere–ocean interaction during El Niño. Part I: The North Pacific Ocean. *Journal of Climate*, *5*(9), 944–958. https://doi.org/10.1175/1520-0442(1992)005<0944:MAIDEN>2.0.CO;2

Alexander, M. A., Bladé, I., Newman, M., Lanzante, J. R., Lau, N.-C., & Scott, J. D. (2002). The atmospheric bridge: The influence of ENSO teleconnections on air-sea interaction over the global oceans. *Journal of Climate*, *15*(16), 2205–2231. https://doi.org/10.1175/1520-0442(2002)015<2205:TABTIO>2.0.CO;2

Barsugli, J. J., & Battisti, D. S. (1998). The basic effects of atmosphere–ocean thermal coupling on midlatitude variability. *Journal of the Atmospheric Sciences*, *55*(4), 477–493. https://doi.org/10.1175/1520-0469(1998)055<0477:TBEOAO>2.0.CO;2

Bladé, I. (1999). The influence of midlatitude ocean–atmosphere coupling on the low-frequency variability of a GCM. Part II: Interannual variability induced by tropical SST forcing. *Journal of Climate*, *12*(1), 21–45. https://doi.org/10.1175/1520-0442(1999)012<0021:TIOMOA>2.0.CO;2

Branstator, G. (1990). Low-frequency patterns induced by stationary waves. *Journal of the Atmospheric Sciences*, *47*(5), 629–649. https://doi.org/10.1175/1520-0469(1990)047<0629:LFPIBS>2.0.CO;2

Cayan, D. R. (1992a). Latent and sensible heat flux anomalies over the northern oceans: The connection to monthly atmospheric circulation. *Journal of Climate*, *5*(4), 354–369. https://doi.org/10.1175/1520-0442(1992)005<0354:LASHFA>2.0.CO;2

Cayan, D. R. (1992b). Latent and sensible heat flux anomalies over the northern oceans: Driving the sea surface temperature. *Journal of Physical Oceanography*, *22*(8), 859–881. https://doi.org/10.1175/1520-0485(1992)022<0859:LASHFA>2.0.CO;2

Deser, C., & Timlin, M. S. (1997). Atmosphere–ocean interaction on weekly timescales in the North Atlantic and Pacific. *Journal of Climate*, *10*(3), 393–408. https://doi.org/10.1175/1520-0442(1997)010<0393:AOIOWT>2.0.CO;2

Horel, J. D., & Wallace, J. M. (1981). Planetary-scale atmospheric phenomena associated with the Southern Oscillation. *Monthly Weather Review*, *109*(4), 813–829. https://doi.org/10.1175/1520-0493(1981)109<0813:PSAPAW>2.0.CO;2

Jin, F., Pan, L., & Watanabe, M. (2006a). Dynamics of synoptic eddy and low-frequency flow interaction. Part I: A linear closure. *Journal of the Atmospheric Sciences*, *63*(7), 1677–1694. https://doi.org/10.1175/JAS3715.1

Jin, F., Pan, L., & Watanabe, M. (2006b). Dynamics of synoptic eddy and low-frequency flow interaction. Part II: A theory for low-frequency modes. *Journal of the Atmospheric Sciences*, *63*(7), 1695–1708. https://doi.org/10.1175/JAS3716.1

Kim, M., Yoo, C., Sung, M.-K., & Lee, S. (2021). Classification of wintertime atmospheric teleconnection patterns in the Northern Hemisphere. *Journal of Climate*, *34*(5), 1847–1861. https://doi.org/10.1175/JCLI-D-20-0339.1

Kosaka, Y., Nakamura, H., Watanabe, M., & Kimoto, M. (2009). Analysis on the dynamics of a wave-like teleconnection pattern along the summertime Asian jet based on a reanalysis dataset and climate model simulations. *J. Meteor. Soc. Japan*, *87*(3), 561–580. https://doi.org/10.2151/jmsj.87.561

Kushnir, Y., Robinson, W., Bladé, I., Hall, N., Peng, S., & Sutton, R. (2002). Atmospheric GCM response to extratropical SST anomalies: Synthesis and evaluation. *Journal of Climate*, *15*(16), 2233–2256. https://doi.org/10.1175/1520-0442(2002)015%3C2233:AGRTES%3E2.0.CO;2

Lau, N.-C. (1988). Variability of the observed midlatitude storm tracks in relation to low-frequency changes in the circulation pattern. *Journal of the Atmospheric Sciences*, *45*(19), 2718–2743. https://doi.org/10.1175/1520-0469(1988)045<2718:VOTOMS>2.0.CO;2

Lau, N.-C., & Holopainen, E. O. (1984). Transient eddy forcing of the time-mean flow as identified by geopotential tendencies. *Journal of the Atmospheric Sciences*, *41*(3), 313–328. https://doi.org/10.1175/1520-0469(1984)041<0313:TEFOTT>2.0.CO;2

Lau, N.-C., & Nath, M. J. (1996). The role of the "atmospheric bridge" in linking tropical Pacific ENSO events to extratropical SST anomalies. *Journal of Climate*, *9*(9), 2036–2057. https://doi.org/10.1175/1520-0442(1996)009<2036:TROTBI>2.0.CO;2

Lau, N.-C., & Nath, M. J. (2001). Impact of ENSO on SST variability in the North Pacific and North Atlantic: Seasonal dependence and role of extratropical sea-air coupling. *Journal of Climate*, *14*(13), 2846–2866. https://doi.org/10.1175/1520-0442(2001)014<2846:IOEOSV>2.0.CO;2

Leathers, D. J., Yarnal, B., & Palecki, M. A. (1991). The Pacific/North American teleconnection pattern and United States climate. Part I: Regional temperature and precipitation associations. *Journal of Climate*, *4*(5), 517–528. https://doi.org/10.1175/1520-0442(1991)004<0517:TPATPA>2.0.CO;2

Lee, J., Sperber, K. R., Gleckler, P. J., Bonfils, C. J., & Taylor, K. E. (2019). Quantifying the agreement between observed and simulated extratropical modes of interannual variability. *Climate Dynamics*, *52*(7–8), 4057–4089. https://doi.org/10.1007/s00382-018-4355-4

Martineau, P., Nakamura, H., Kosaka, Y., & Yamamoto, A. (2020). Importance of a vertically tilting structure for energizing the North Atlantic Oscillation. *Scientific Reports*, *10*(1), 1–10. https://doi.org/10.1038/s41598-020-69551-5

Mori, M. (2024a). MIROC6-AGCM dataset for "Northern Hemisphere winter atmospheric teleconnections are intensified by extratropical ocean-atmosphere coupling" (Version 1.0) [Dataset]. *Zenodo*. https://doi.org/10.5281/zenodo.10565870

Mori, M. (2024b). MIROC6-AGCM dataset for "The influence of Extratropical Ocean on the PNA Teleconnection: Role of Atmosphere-Ocean Coupling" (Version 1.0) [Dataset]. *Zenodo*. https://doi.org/10.5281/zenodo.12154898

Mori, M., Kosaka, Y., Taguchi, B., Tokinaga, H., Tatebe, H., & Nakamura, H. (2024). Northern Hemisphere winter atmospheric teleconnections are intensified by extratropical ocean-atmosphere coupling. *Communications Earth & Environment*, *5*(1), 124. https://doi.org/10.1038/s43247-024-01282-1

Mori, M., & Watanabe, M. (2008). The growth and triggering mechanisms of the PNA: A MJO-PNA coherence. *J. Meteor. Soc. Japan*, *86*(1), 213–236. https://doi.org/10.2151/jmsj.86.213

Nakamura, H., Tanaka, M., & Wallace, J. M. (1987). Horizontal structure and energetics of Northern Hemisphere wintertime teleconnection patterns. *Journal of the Atmospheric Sciences*, *44*(22), 3377–3391. https://doi.org/10.1175/1520-0469(1987)044<3377:HSAEON>2.0.CO;2

Palmer, T. N. (1999). A nonlinear dynamical perspective on climate prediction. *Journal of Climate*, *12*(2), 575–591. https://doi.org/10.1175/1520-0442(1999)012<0575:ANDPOC>2.0.CO;2

Simmons, A., Wallace, J., & Branstator, G. (1983). Barotropic wave propagation and instability, and atmospheric teleconnection patterns. *Journal of the Atmospheric Sciences*, *40*(6), 1363–1392. https://doi.org/10.1175/1520-0469(1983)040<1363:BWPAIA>2.0.CO;2

Snedecor, G. W., & Cochran, W. G. (1989). *Statistical methods* (8th Ed.). Iowa State University Press.

Tatebe, H., Ogura, T., Nitta, T., Komuro, Y., Ogochi, K., Takemura, T., et al. (2019). Description and basic evaluation of simulated mean state, internal variability, and climate sensitivity in MIROC6. *Geoscientific Model Development*, *12*(7), 2727–2765. https://doi.org/10.5194/gmd-12-2727-2019

Taylor, K., Williamson, D., & Zwiers, F. (2000). The sea surface temperature and sea-ice concentration boundary conditions for AMIP II simulations. *PCMDI Rep*, *60*, 25.

Trenberth, K. E., Branstator, G. W., Karoly, D., Kumar, A., Lau, N. C., & Ropelewski, C. (1998). Progress during TOGA in understanding and modeling global teleconnections associated with tropical sea surface temperatures. *Journal of Geophysical Research*, *103*(C7), 14291–14324. https://doi.org/10.1029/97JC01444

Wallace, J. M., & Gutzler, D. S. (1981). Teleconnections in the geopotential height field during the Northern Hemisphere winter. *Monthly Weather Review*, *109*(4), 784–812. https://doi.org/10.1175/1520-0493(1981)109<0784:TITGHF>2.0.CO;2

References From the Supporting Information

Okajima, S., Nakamura, H., & Kaspi, Y. (2022). Energetics of transient eddies related to the midwinter minimum of the North Pacific storm-track activity. *Journal of Climate*, *35*(4), 1137–1156. https://doi.org/10.1175/JCLI-D-21-0123.1

Tanaka, S., Nishii, K., & Nakamura, H. (2016). Vertical structure and energetics of the western Pacific teleconnection pattern. *Journal of Climate*, *29*(18), 6597–6616. https://doi.org/10.1175/JCLI-D-15-0549.1